國立交通大學

電信工程學系碩士班

碩士論文

超寬調諧範圍之電壓控制振盪器設計

An Ultra-Wide Tuning - Range VCO

研 究 生：蘇國政

指導教授：唐震寰　教授

中華民國九十九年七月

超寬調諧範圍之電壓控制震盪器設計

An Ultra-Wide Tuning - Range VCO

研究生：蘇國政　　Student：Kuo-Cheng Su

指導教授：唐震寰　教授　　Advisor：Jenn-Hwan Tarng

國立交通大學

電信工程學系碩士班

碩士論文

A Thesis
Submitted to Department of Communication Engineering
College of Electrical Engineering and Computer Science
National Chiao Tung University
in Partial Fulfillment of the Requirements
for the Degree of
Master
in

Communication Engineering

July 2010

Hsinchu, Taiwan, Republic of China

中華民國九十九年七月

超寬調諧範圍之電壓控制振盪器設計

研究生：蘇國政　　　　　　　　　　指導教授：唐震寰

國立交通大學

電信工程學系 碩士班

摘要

為了增加壓控振盪器(VCO)的調諧範圍，我們通常會使用差動式主動電感來取代單端式主動電感，因為差動式主動電感使用較少的電晶體，導致寄生電容較小，因此使用差動式主動電感可達到較寬的調諧頻率。但在差動式主動電感中，增加可調頻率範圍會造成整體電路的電流降低，而 VCO 中的負阻元件也將因為電流不足而無法正常工作，可調頻率範圍約只能到達 3GHz 的頻寬，tuning range也只有約 120%。本篇論文提出一個可調範圍達 5GHz 頻寬的 VCO。此 VCO 使用差動式主動電感的架構，並額外加上一個回授電阻於主動式電感中，該回授電阻可限制可調電導的最小值，整體電路的電流不會因為電導值過小而不足，因此 VCO 的調諧範圍可大幅增加。本論文使用台積電 0.18μm 1P6M 製程技術實現，量測結果顯示輸出頻率為 0.5GHz 到 5.6GHz。可調頻率達 5GHz，tuning range 為 165%，相位雜訊在 1MHz offset時為-94 到-99dBc/Hz。使用此主動式電感，整體 VCO 的面積只有 175 x 170 μm^2 。

An Ultra-Wide Tuning-Range VCO in 0.18 μm CMOS

Student：Kuo-Cheng Su　　Advisor：Dr. Jenn-Hwan Tarng

Department of Communication Engineering
National Chiao Tung University

Abstract

In order to increase the frequency tuning range of a voltage-controlled oscillator (VCO), single-ended active inductors are usually replaced by differential active inductors, which need less number of transistors to yield smaller parasitic capacitance. However, the differential active inductors lower the overall current and may lead VCO's negative resistance to be out of function, which still limits the frequency tuning range. In this thesis, a feedback resistor is added to limit the minimum conductance of the active inductor to achieve an ultra-wide tuning range VCO of 5 GHz. The proposed circuit is implemented by the TSMC 0.18μm 1P6M process technology, and the measurement result of the proposed VCO can be tuned from 0.5 GHz to 5.6 GHz. Its frequency tuning range is 165%. The phase noise ranges from -94 to -99 dBc/Hz at a 1-MHz offset. The die area of the VCO is 175 x 170 μm^2.

誌　　謝

在碩士班研究的這二年歲月，首先要感謝我的指導教授　唐震寰教授並致上我最誠摯的謝意。感謝老師在專業的通訊領域中，給予我不斷的指導與鼓勵，並賦予了實驗室豐富的研究資源與環境，使得這篇碩士論文能夠順利完成。同時，亦感謝口試委員國立交通大學　張翼教授及中華大學　田慶誠教授對於論文內容所提出的寶貴建議及指導，在此致上最誠懇的謝意。

其次，要感謝波散射與傳播實驗室的學長們—佩宗、標哥、俊諺、雅仲、振銘、廣琪、兆凱、明宗，以及學弟們—佳迪、昌喆、阿順、啟宏，還有一起奮鬥的好夥伴—豪哥、康馬、Poter、阿諾、阿凱，除了在研究上給我的幫助與意見，讓我獲益良多，同時讓我擁有兩年多彩多姿的生活。另外，也要感謝助理—梁麗君小姐，在實驗室上的協助和籌劃每次的美食聚餐饗宴。

最後，要感謝的就是我最親愛的家人。他們在我求學過程中，一路陪伴著我，給予我最溫馨的關懷與鼓勵，讓我在人生的過程裡得到快樂，更讓我可以專心於研究工作中而毫無後顧之憂。

鑒此，謹以此篇論文獻給所有關心我的每一個人。

蘇國政　誌予

九十九年八月

Table of Contents

Chapter 3 Advanced Designs of Related Works 30

Chapter 4 Proposed Wide tuning range VCO 31

Chapter 5 Conclusion 44

List of Tables

List of Figures

Chapter 1 Introduction

1.1 Background and Problems

In recent years, the development of several kinds of new communication techniques is expected to provide high data rate, wide range and high speed communications in wireless area networks [1]. As the advancement of wireless communication systems, transmission distance and data rate are growing rapidly. The design of high performance radio frequency (RF) transceivers is an aspiration target.

At present, RF transceivers have been widely implemented by SiGe, GaAs or HBT processes due to the high performance at high frequency. However, the system cost will remain high because those processes are not compatible with the silicon process. Thus, the CMOS technology is an attractive process to meet the low cost requirement in RF transceivers.

Among function blocks of a RF transceiver as shown in Fig 1.1, the voltage controlled oscillator (VCO) is used to provide clean, stable, and precise carrier signals for frequency translation in wireless transceivers. Because the purity (phase noise) of local signal which is generated by the VCO will dominate the performance of the system, the design of high performance VCO is an urgent and momentous subject. In the design of VCOs, there are several common goals, such as low phase noise, low power consumption, low cost, satisfactory output power, and wide tuning range. In the past, the tuning range was not taken seriously. However, the fast-growing market in wireless communications has lead to multiple wireless standards. Therefore, the wide tuning range VCO is essential. A device can be used for multiple wireless standards will reduce the cost of manufacturing. However, according to the well-known Leeson's model of phase noise [2], the phase noise and tuning range usually formed a key tradeoff in the circuit design of VCOs. Hence, designing a VCO that satisfies the requirements described above is a challenging issue.

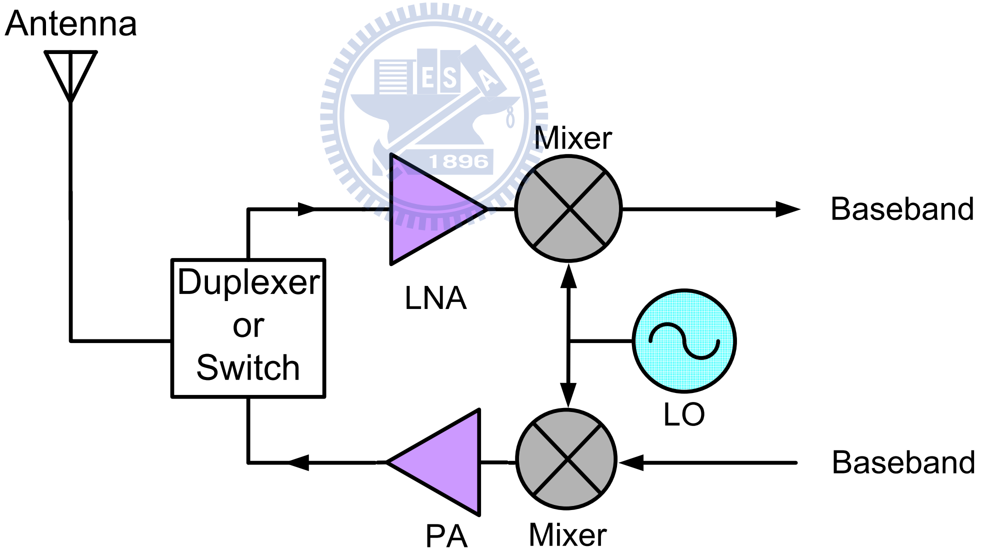

Figure 1.1 Block diagram of a typical RF front-end transceiver

1.2 Related Works and Motivation

In recent years, rapid growth of wireless communication markets has led to multiple wireless standards. These wireless standards may coexist on the same frequency; therefore, the hardware reused for multiple standards becomes an important issue. In order to solve this problem, the wide tuning range VCO is essential. In the past research, LC-tank VCOs with spiral inductors and varactors are the most used for circuit implementation at radio frequencies. This structure of the tuning frequency depends entirely on the varactor's tunable range; therefore, subject to the influence of traditional CMOS process, the tuning range is limited to less than 30% [3]- [5] making it unattractive for wideband applications. Many ways have been proposed to improve the tuning range of the LC-tank VCO by switched capacitors [6], [7]. To operate at multiple frequencies, a number of switched -capacitor converters for VCO are used. Though the tuning range can be improved, the overall circuit area has increased considerably.

To overcome the increase in chip size, the structure of active inductors has been introduced [8]. An active inductor can be realized by using two gyrators and a capacitor. By rotating the phase to 180- degree, the capacitor shows inductance. Using this active inductor to replace the spiral inductor of LC- tank VCO can effectively reduce the chip area. However, this is a one-port inductor topology, so to completely replace the spiral inductor, the active inductor must use more than four transistors, and using more transistors will lead to the increased of the noise on the circuit significantly. In conclusion, obtaining a wide tuning range at the small chip size and maintain appropriate phase noise becomes a bottleneck to design.

In this thesis, using differential active inductors and adding a feedback resistor to the tunable conductance can achieve the effect of broadband and smaller chip area. In addition, the capacitor at the output can improve the phase noise.

1.3 Thesis Organization

There are five chapters in this thesis. Chapter 2 describes the basic concepts of VCO design. In chapter 3, some advanced active inductor topologies are reviewed. In chapter 4, we design the ultra wide tuning range VCO with simulated and measured results. In chapter 5, the conclusion is drawn.

Chapter 2 *Design Basics of CMOS VCO*

2.1 Fundamental Characteristics of VCO

In the modern wireless communication system, the VCO is an important block in the building block of a radio frequency. It is used as a local oscillator to up-conversion or down-conversion signals. In general, the VCO is a spontaneous circuit. However, how is an output of precise periodic waveform without the input signal in the circuit generated?

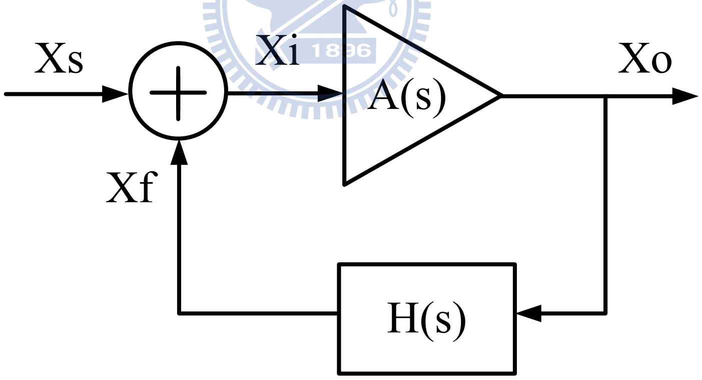

Figure 2.1 Feedback model of a VCO.

Fig. 2.1 shows the block diagram of the feedback model. The transfer function of the output/input is given as

$$\frac{Xo(s)}{Xs(s)} = \frac{A(s)}{1 - A(s)H(s)} \tag{2-1}$$

When open loop gain is

$$Ao(s) = A(s)H(s) \tag{2-2}$$

with

$$\left|Ao(\omega_0)\right| = 1 \;\; \& \;\; \angle Ao(j\omega_0) = 0 \tag{2-3}$$

The feedback system will start oscillating, and maintain the certain amplitude of output signal. This is called Barkhauen criterion, where ω_0 is the radian frequency of oscillation. The Barkhauen criterion of the feedback circuit is a necessary condition but not sufficient. In order to ensure oscillation in the presence of temperature and process variations, we typically choose the loop gain to be at least twice or three times the required value.

2.2 LC Tank VCO

Fig. 2.2 shows the series resonant circuit and the parallel resonant circuit with input impedance Z$_{in}$ given by

$$Z_{in} = R + j\omega L + \frac{1}{j\omega C} \quad \text{(series resonant circuit)} \tag{2-4a}$$

and

$$Z_{in} = \frac{1}{1/R + 1/j\omega L + j\omega C} \quad \text{(parallel resonant circuit)} \tag{2-4b}$$

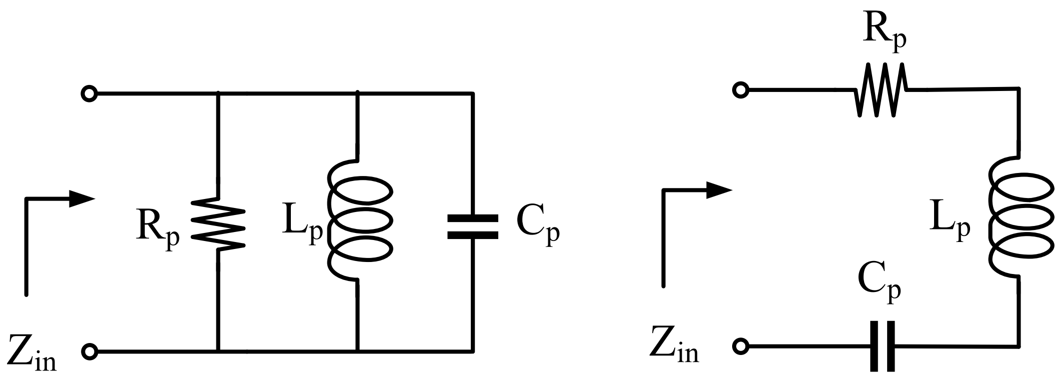

(a) (b)

Figure 2.2 (a) Parallel resonator (b) series resonator.

In the parallel resonator, the LC tank will start oscillating with

$$\omega L = \frac{1}{\omega C} \tag{2-5}$$

The input impedance and oscillating frequency are

$$Z_{in} = R_p \tag{2-6}$$

$$\omega = \omega_0 = \frac{1}{\sqrt{LC}} \tag{2-7}$$

From the analysis of the LC-tank, the Q (quality) factor is given as

$$Q = \omega \frac{average\ enegy\ store}{average\ energy\ loss\ \ per\ cycle} \tag{2-8}$$

2.3 Negative-Resistor for LC tank VCO

In fact, the LC-tank VCO can not maintain a stable output waveform, because the equivalent resistance R_p will result in the degradation of the waveform (Fig. 2.3a). Therefore, we need the active circuit to compensate the energy loss (Fig. 2.3b).

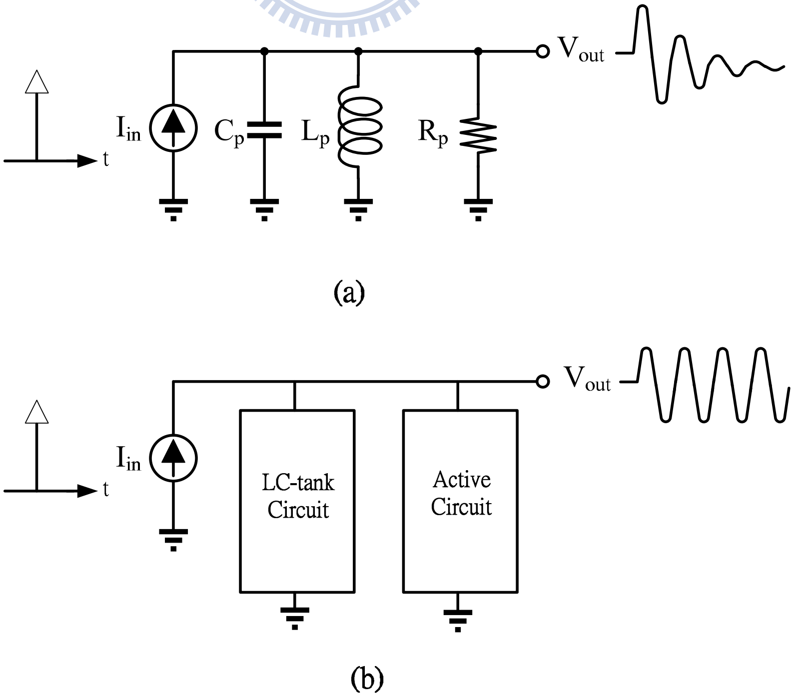

(a)

(b)

Figure 2.3 (a) Decaying impulse response of a tank, (b) addition of active circuit to cancel loss in the LC-Tank

This active circuit is called the "negative resistance." The negative resistance provides an equivalent resistance $-R_p$. It can cancel the equivalent resistance R_p resulting in the indefinite oscillation of the LC-tank. How do we generate the negative resistance device? In the device, when the current decreases as the voltage increases, this device is called the "negative resistance." We can use two transistors and the feedback system to achieve negative resistance. Fig. 2.4 shows the negative resistance.

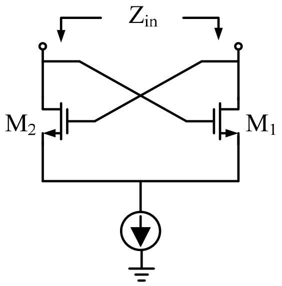

Figure 2.4 The negative resistance cell with two transistors.

Using the small signal analysis, the input impedance can be expressed as

$$Z_{in} = -\left(\frac{1}{g_{m1}} + \frac{1}{g_{m2}}\right) = -\frac{2}{g_m} \quad (\text{if } g_{m1}=g_{m2}=g_m) \tag{2-9}$$

With a negative resistance available, we can now construct an oscillator as illustrated in Fig. 2.5. The oscillator starts oscillation conditions for

$$R_p - \frac{2}{g_m} \geq 0 \tag{2-10}$$

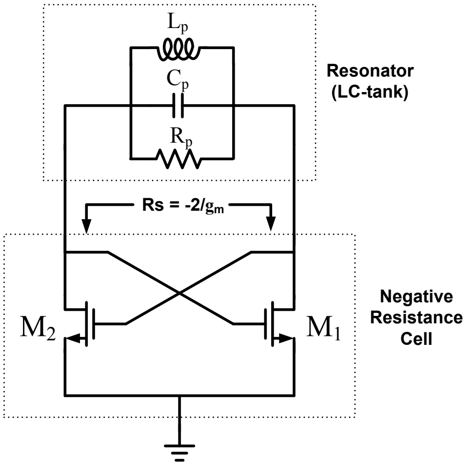

Figure 2.5 The negative resistance in parallel on the LC-tank circuit.

2.4 Phase Noise

One of the most important characteristic of VCOs is phase noise. We can know the impact of the next level by phase noise parameters. An ideal sine wave of the spectrum is a pulse function (Figure 2.6 (a)). The actual circuit contains a variety of noise lead to the oscillator output signal frequency spectrum curves like a skirt (Figure 2.6 (b)).

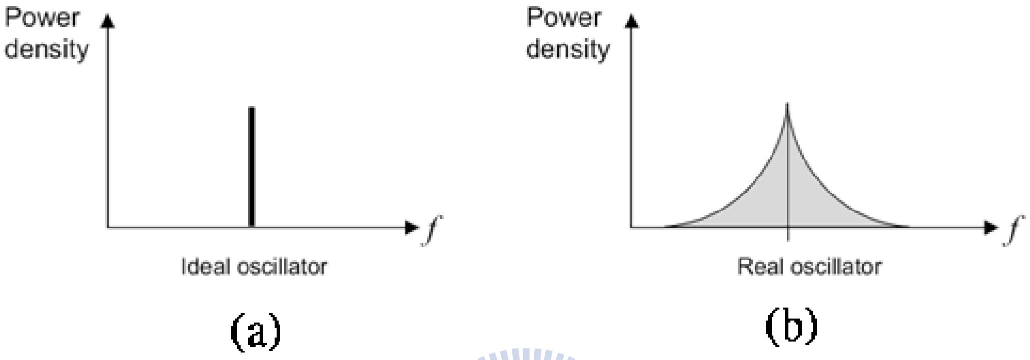

Figure 2.6 (a) Frequency spectrum of ideal oscillators (b) Frequency spectrum of real oscillators

An ideal sinusoidal wave form is defined as

$$V(t) = A\cos(\omega_0 t + \phi) \qquad (2\text{-}11)$$

where A is the oscillated amplitude, ω_0 is oscillated frequency and ϕ is a random phase. The waveform function should be

$$V(t) = A(t) f(\omega_0 t + \phi(t)) \qquad (2\text{-}12)$$

where the oscillated amplitude $A(t)$ and phase $\phi(t)$ are functions of time t, the function f has the period of 2π. The jitter can cause the amplitude fluctuation and phase fluctuation in a VCO. Mostly, the amplitude fluctuation can be neglected due to the voltage limiter or nonlinearity effect of the circuits, but the phase fluctuation can not..

Frequency fluctuations are usually characterized by the single sideband noise spectral density normalized to the carrier signal power (Fig. 2.6). It is defined as

$$L(f_c,\Delta f)=10\log\left[\frac{P_{sideband}(f_c+\Delta f,1Hz)}{P_{carrier}}\right] \tag{2-13}$$

and has units of decibels below the carrier per hertz (dBc/Hz). $P_{carrier}$ is the carrier signal power at the carrier frequency f_C and $P_{sideband}(f_c+\Delta f, 1\ Hz)$ denotes the single sideband power at the offset Δf from the carrier f_C at a measurement bandwidth of 1 Hz.

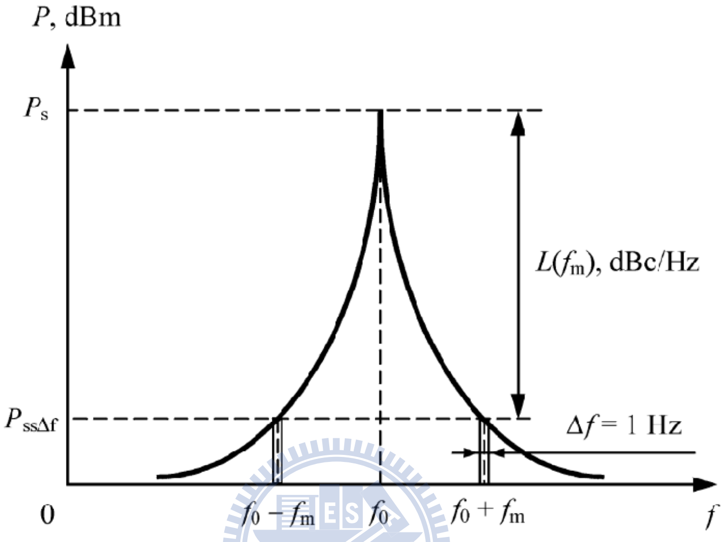

Figure 2.7 Oscillator output power spectrum

The typical oscillator output power spectrum is shown in Fig. 2.7. The noise distribution on each side of the oscillator signal is subdivided into a larger number of strips of width Δf located at the distance f_m away from the single. It should be noted that, generally, the spectrum of the output single consists of the phase noise components. Hence, to measure the phase noise close to the carrier frequency, one needs to make sure that any contributions of parasitic amplitude modulation to the oscillator output noise spectrum are negligible compared with those from frequency modulation. The single sideband phase noise $L(f_m)$ usually given logarithmically is defined as the ratio of signal power $P_{ss\Delta f}$ in one phase modulation sideband per bandwidth Δf=1 Hz, at an offset f_m away from the carrier, to the total signal power P_s.

Time invariant model

In this section, phase noise analysis is described by using time invariant model. Time invariant means whenever noise sources injection, the phase noise in VCO is the same. In the other words, phase shift of VCO caused by noise is the same in any time. Therefore, it's no need to consider when the noise is coming. Suppose oscillator is consists of amplifier and resonator. The transfer function of a band-pass resonator is written as

$$H\left(j\omega\right)=\frac{j\omega\frac{1}{RC}}{\frac{1}{LC}+j\omega\frac{1}{RC}-\omega^{2}} \tag{2-14}$$

The transfer function of a common band-pass is written as

$$H\left(j\omega\right)=\frac{j\omega\frac{\omega_0}{Q}}{\omega_0^{2}+j\omega\frac{\omega_0}{Q}-\omega^{2}} \tag{2-15}$$

Compare equation (2-14) with (2-15). Thus,

$$\omega_0=\frac{1}{LC} \quad \text{and} \quad Q=\omega_0 RC \tag{2-16}$$

The frequency $\omega=\omega_0+\Delta\omega$ which is near oscillator output frequency. If $\omega_0 \gg \Delta\omega$, we can use Taylor expansion for only first and second terms. Hence

$$H\left(j\omega\right)\approx 1+\frac{2}{j\frac{\omega_0}{Q}}\cdot\Delta\omega \tag{2-17}$$

The close-loop response of oscillator is expressed by

$$G\left(j\omega\right)=\frac{1}{1-H\left(j\omega\right)}\approx\frac{-j\frac{\omega_0}{Q}}{2\cdot\Delta\omega} \tag{2-18}$$

When input noise density is $S_i\left(\omega\right)$, the output noise density is

$$S_0(\omega)=S_i(\omega)\left|G(\omega)\right|^2=FkT\left(\frac{\omega_0}{2Q\Delta\omega}\right)^2 \tag{2-19}$$

The above equation is double sideband noise. The phase noise faraway center frequency $\Delta\omega$ can be expressed by

$$L(\Delta\omega)=10\log\left[\frac{2FkT}{P_S}\cdot\left(\frac{\omega_0}{2Q\Delta\omega}\right)^2\right] \tag{2-20}$$

Where F is empirical parameter ("often called the device excess noise number"), k is Boltzman' s constant, T is the absolute temperature, P_S is the average power dissipated in the resistive part of the tank, ω_0 is the oscillation frequency, and Q is the effective quality factor of the tank with all the loading in place(also known as loaded Q). From equation (2-20), increasing power consumption and higher Q factor can get better phase noise. Increasing power consumption means increasing the power of amplifier. This method will decrease noise figure (NF) and improve phase noise.

From, equation (2-20), we can briefly understand phase noise. But the equation and actual measured results are different. The VCO spectrum is shown as Fig. 2.7. The phase noise equation can be modified as the same as equation (2-34) that is called Lesson's model [9].

$$L(\Delta\omega)=10\log\left\{\frac{2FKT}{P_S}\cdot\left[1+\left(\frac{\omega_0}{2Q\Delta\omega}\right)^2\right]\cdot\left[1+\frac{\Delta\omega_{1/f^3}}{|\Delta\omega|}\right]\right\} \tag{2-21}$$

These modifications, due to Leeson, consist of a factor to account for the increased noise in the $1/(\Delta\omega)^2$ region, an additive factor of unity (inside the braces) to account for the noise floor, and a multiplicative factor (the term in the second set of parentheses) to provide a $1/|\Delta\omega|^3$ behavior at sufficiently small offset frequencies. With these modifications, the phase-noise spectrum appears as in Fig. 2.8.

It is important to note that the factor F is an empirical fitting parameter and therefore must be determined from measurements, diminishing the predictive power of the phase-noise equation. Furthermore, the model asserts that $\Delta\omega_{1/f^3}$, the boundary between the $1/(\Delta\omega)^2$ and $1/|\Delta\omega|^3$ regions, is precisely equal to the $1/f$ corner of device noise. However, measurements frequently show no such equality, and thus one must generally treat $\Delta\omega_{1/f^3}$ as an empirical fitting parameter as well. Also, it is not clear what the corner frequency will be in the presence of more than one noise source with $1/f$ noise contribution. Last, the frequency at which the noise flattens out is not always equal to half the resonator bandwidth, $\omega_0/2Q$. Both the ideal oscillator model and the Leeson model suggest that increasing resonator Q and signal amplitude are ways to reduce phase noise. The Leeson model additionally introduces the factor F, but without knowing precisely what it depends on, it is difficult to identify specific ways to reduce it. The same problem exists with $\Delta\omega_{1/f^3}$ as well. Last, blind application of these models has periodically led to earnest but misguided attempts to use active circuits to boost Q. Sadly, increases in Q through such means are necessarily accompanied by increases in F as well, preventing the anticipated improvements in phase noise. Again, the lack of analytical expressions for F can obscure this conclusion, and one continues to encounter various doomed oscillator designs based on the notion of active Q boosting.

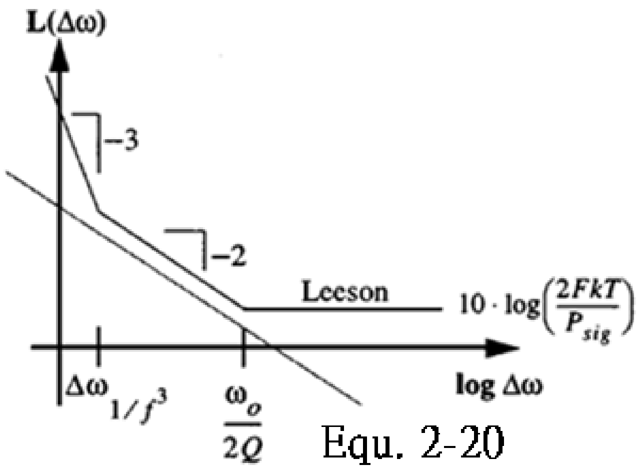

Figure 2.8 Phase noise: Leeson versus (2-20).

Time Variant

In the general case, multiple noise sources affect the phase and amplitude of an oscillator. This chapter begins by investigating the effect of a single noise source on the amplitude and phase of the oscillator.

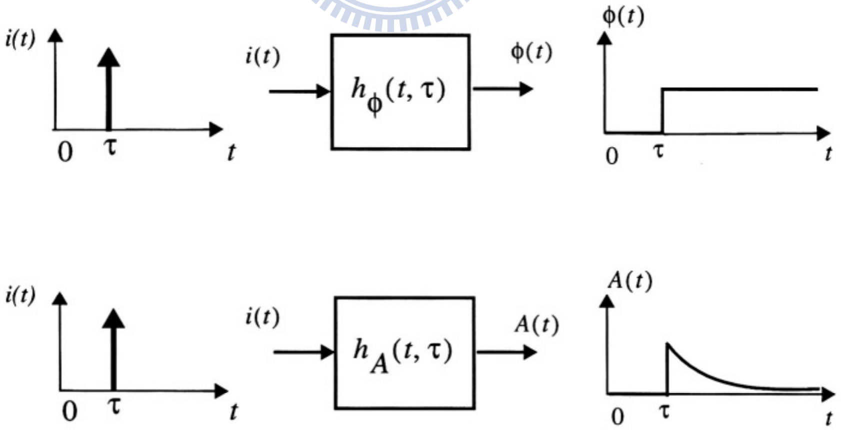

Figure 2.9 Equivalent systems for phase and amplitude

Since each input source generally affects both amplitude and phase, a pair of equivalent systems, one each for amplitude and phase, can be defined. Each system can be viewed as a single-input, single-output system as shown in Fig. 2.9. The input of each system in Fig. 2.9 is a perturbation current (or voltage) and the outputs are the excess phase, ϕ(t), and amplitude, *A(t)*. Both systems shown in Fig. 2.9 are time-variant as shown by the following examples.

The first example is an ideal parallel *LC* tank oscillating with voltage amplitude, as shown in Fig. 2.10. If one injects an impulse of current at the voltage maximum, only the voltage across the capacitor changes; there is no effect on the current through the inductor. Therefore, the tank voltage changes instantaneously, as shown in Fig. 2.10. Assuming a voltage- and time-invariant capacitor, the instantaneous voltage change ΔV is given by

$$\Delta V = \frac{\Delta q}{C_{total}} \tag{2-22}$$

where Δq is the total charge injected by the current impulse and C_{total} is the total capacitance in parallel with the current source. It can be seen from Fig. 2.10 that the resultant change in *A*(*t*) and ϕ(t) is time dependent. In particular, if the impulse is applied at the peak of the voltage across the capacitor, there will be no phase shift and only an amplitude change will result, as shown in Fig. 2.10(a). On the other hand, if this impulse is applied at the zero crossing, it has the maximum effect on the excess phase, ϕ(t), and the minimum effect on the amplitude, as depicted in Fig. 2.10(b).

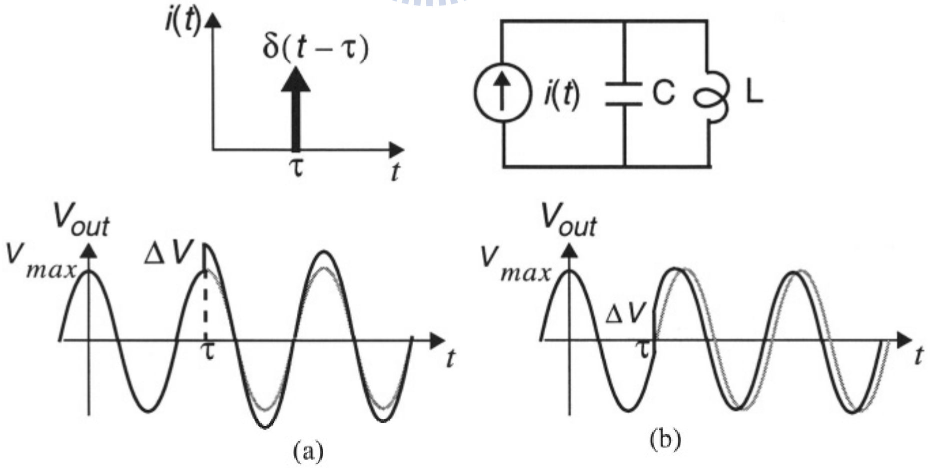

Figure 2.10 Impulse response of an ideal LC oscillator

To emphasize the generality of this time-variance, consider two more examples. The relaxation oscillator known as the Bose oscillator is shown in Fig. 2.11. It consists of a Schmitt-trigger inverter and an RC circuit. The hysteresis in the transfer function of the inverter and the RC time constant determine the frequency of oscillation. The resulting capacitor voltage waveform is shown with a solid line in Fig. 2.12.

As before, imagine an impulsive current source in parallel with the capacitor, injecting charge at t=τ, as shown in Fig. 2.11. All of the injected charge goes into the capacitor and changes the voltage across it instantaneously. This voltage change, ΔV, results in a phase shift, Δϕ, as shown in Fig. 2.12. As can be seen from Fig. 2.12, for a small area of the current impulse (injected charge), the resultant phase shift is proportional to the voltage change, ΔV, and hence to the injected charge, Δq. Therefore, Δϕ can be written as

$$\Delta\phi = \Gamma(\omega_0\tau)\frac{\Delta V}{V_{\max}} = \Gamma(\omega_0\tau)\frac{\Delta q}{q_{\max}} \qquad \Delta q \ll q_{\max} \tag{2-23}$$

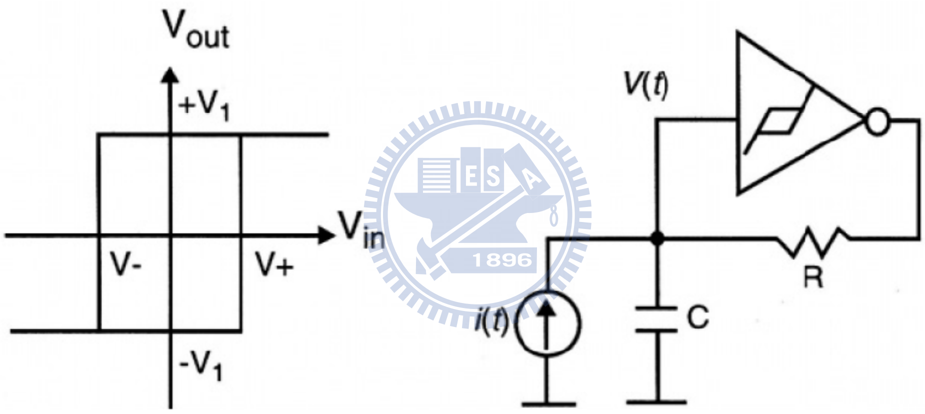

Figure 2.11 Bose oscillator with parallel perturbation current source

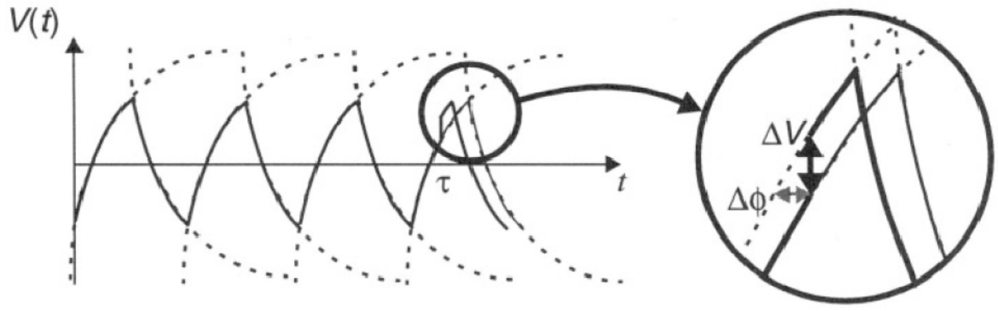

Figure 2.12 The waveform of the Bose oscillator

where V_{max} is the voltage swing across the capacitor and $q_{max}=C_{node}V_{max}$ is the maximum charge swing. The function, Γ(x) is the time-varying "proportionality factor". It is called the *impulse sensitivity function* (ISF), since it determines the sensitivity of the oscillator to an impulsive input. It is a dimensionless, frequency- and amplitude-independent function periodic in 2π that describes how much phase shift results from applying a unit impulse at any point in time.

In any event, to develop a feel for typical shapes of ISF's, consider two representative examples, first for an *LC* and a ring oscillator in Fig. 2.13(a) and (b).

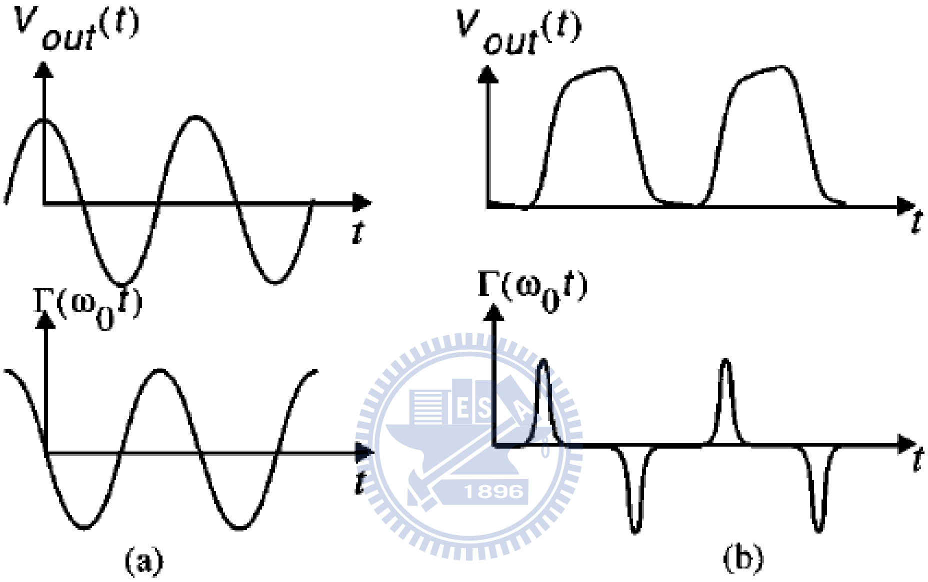

Figure 2.13 Example ISF for (a) *LC* oscillator and (b) ring oscillator.

It is critical to note that the current-to-phase transfer function is linear for small injected charge, even though the active elements may have strongly nonlinear voltage current behavior. It should also be noted that the linearity and time-variance of a system depends on both the characteristics of the system and its input and output variables. The linearization of the current-to-phase system of Fig. 2.9 does not imply linearization of the nonlinearity of the voltage-current characteristics of the active devices. In fact, this nonlinearity affects the shape of the ISF and therefore has an important influence on phase noise, as will be seen shortly.

Noting that the introduced phase shift persists indefinitely, the unity phase impulse response can be easily calculated from (2-23) to be

$$h_{\Phi}(t,\tau)=\frac{\Gamma(\omega_0\tau)}{q_{\max}}u(t-\tau) \tag{2-24}$$

where $u(t)$ is the unit step.

Thanks to linearity, the output excess phase, $\phi(t)$, can be calculated for small charge injections using the superposition integral

$$\phi(t)=\int_{-\infty}^{+\infty}h_{\phi}(t,\tau)i(\tau)d\tau=\int_{-\infty}^{t}\frac{\Gamma(\omega_0\tau)}{q_{\max}}i(\tau)d\tau \tag{2-25}$$

where $i(t)$ represents the input noise current injected into the node of interest. Equation (2-25) is one of the most important results of this section and will be referred to frequently.

The output voltage, $V(t)$, is related to the phase, $\phi(t)$, through a phase modulation process. Thus the complete process by which a noise input becomes an output perturbation in $V(t)$ can be summarized in the block diagram of Fig. 2.14. The essential features of the block diagram of Fig. 2.14 are a modulation by a periodic function, an ideal integration and a nonlinear phase modulation. The complete process thus can be viewed as a cascade of an LTV system that converts current (or voltage) to phase, with a nonlinear system that converts phase to voltage.

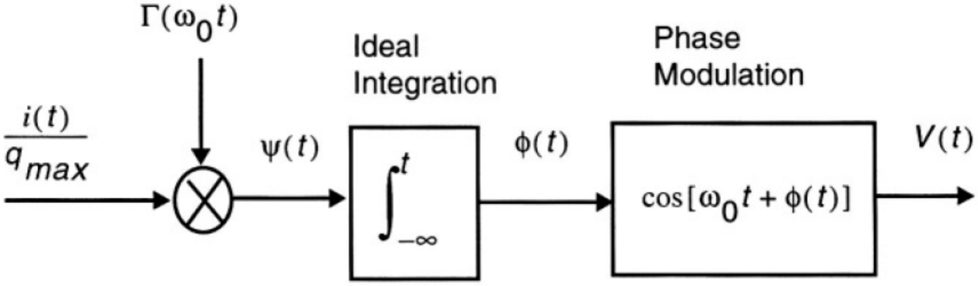

Figure 2.14 The equivalent block diagram of the process.

Since the ISF is periodic, it can be expanded in a Fourier series

$$\Gamma(\omega_0\tau)=c_0+\sum_{n=1}^{\infty}c_n\cos(n\omega_0\tau+\theta_n) \tag{2-26}$$

where the coefficients c_n are real-valued, and θ_n is the phase of the nth harmonic. As will be seen later, θ_n is not important for random input noise and is thus neglected here. Using the expansion in (2-26) for $\Gamma(\omega_0\tau)$ in the superposition integral and exchanging the order of summation and integration, the following is obtained:

$$\phi(t) = \frac{1}{q_{\max}}\left[c_0\int_{-\infty}^{t} i(\tau)d\tau + \sum_{n=1}^{\infty} c_n \int_{-\hbar}^{t} i(\tau)\cos(n\omega_0\tau)d\tau\right] \tag{2-27}$$

Equation (2-27) identifies individual contributions to the total ϕ(t) for an arbitrary input current *i*(*t*) injected into any circuit node, in terms of the various Fourier coefficients of the ISF. The decomposition implicit in (2-27) can be better understood with the equivalent block diagram shown in Fig. 2.15.

Each branch of the equivalent system in Fig. 2.15 acts as a bandpass filter and a downconverter in the vicinity of an integer multiple of the oscillation frequency. For example, the second branch weights the input by c_1, multiplies it with a tone at ω_0 and integrates the product. Hence, it passes the frequency components around ω_0 and downconverts the output to the baseband. As can be seen, components of perturbations in the vicinity of integer multiples of the oscillation frequency play the most important role in determining ϕ(t).

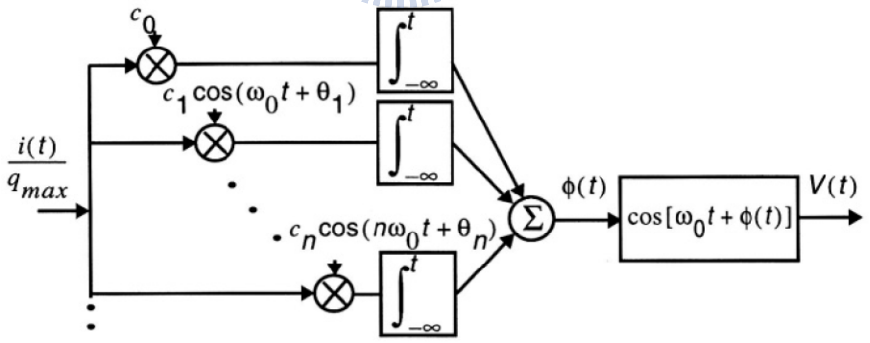

Figure 2.15 The equivalent system for ISF decomposition

To investigate the effect of low frequency perturbations on the oscillator phase, a low frequency sinusoidal perturbation current, *i*(*t*), is injected into the oscillator at a frequency of $\Delta\omega \ll \omega_0$:

$$i(t) = I_0\cos(\Delta\omega t) \tag{2-28}$$

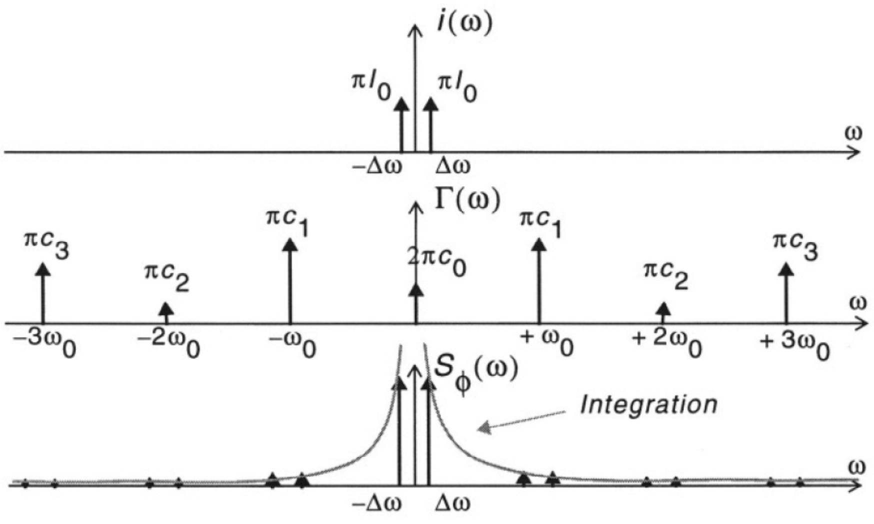

Figure 2.16 Conversion of a low frequency sinusoidal current to phase

where I_0 is the amplitude of $i(t)$. The arguments of all the integrals in (2-27) are at frequencies higher than $\Delta\omega$ and are significantly attenuated by the averaging nature of the integration, except the term arising from the first integral, which involves c_0. Therefore, the only significant term in ϕ(t) will be

$$\phi(t) \approx \frac{I_0 c_0}{q_{\max}} \int_{-\infty}^{t} \cos(\Delta\omega\tau)\,d\tau = \frac{I_0 c_0 \sin(\Delta\omega t)}{q_{\max}\Delta\omega} \qquad \text{(2-29)}$$

As a result, there will be two impulses at $\pm\Delta\omega$ in the power spectral density of ϕ(t), denoted as $S_\phi(\omega)$ as shown in Fig. 2.16.

As another important special case, consider a current at a frequency close to the oscillation frequency given by

$$i(t) = I_1 \cos\left[(\omega_0 + \Delta\omega)t\right] \qquad \text{(2-30)}$$

A process similar to that of the previous case occurs except that the spectrum of $i(t)$ consists of two impulses at $\pm(\omega_0+\Delta\omega)$ as shown in Fig. 2.17. This time the dominant term in (2-27) will be the second integral corresponding to n=l. Therefore, ϕ(t) is given

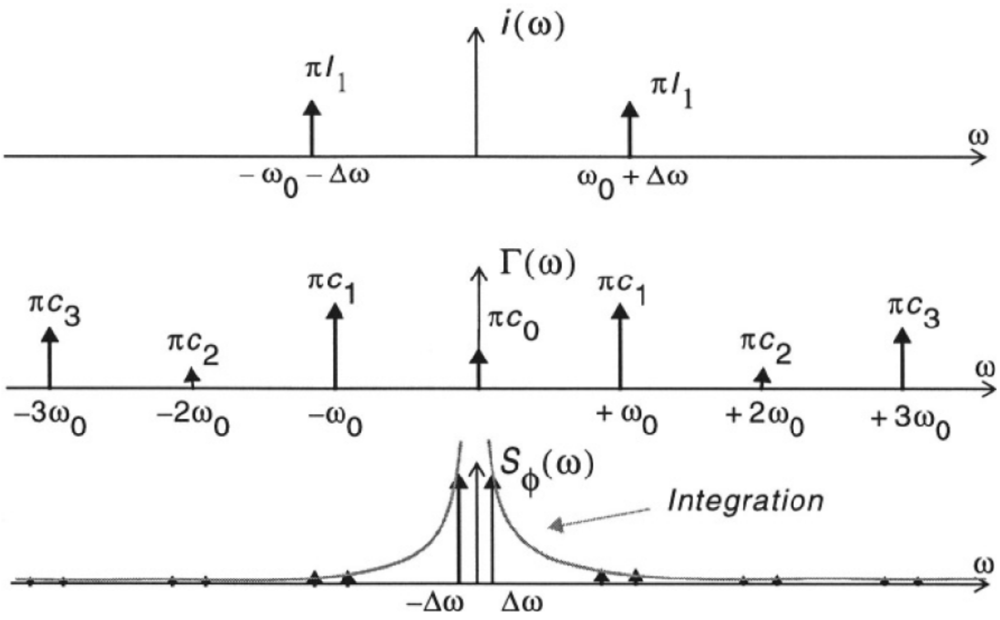

Figure 2.17 Conversion of a tone in the vicinity of ω_0

by

$$\phi(t) \approx \frac{I_1 c_1 \sin(\Delta\omega t)}{2 q_{\max} \Delta\omega} \tag{2-31}$$

which again results in two equal sidebands at $\pm\Delta\omega$ in $S_\phi(\omega)$.

More generally, (2-27) suggests that applying a current, $i(t) = I_n \cos\left[(n\omega_0 + \Delta\omega)t\right]$, close to any integer multiple of the oscillation frequency will result in two equal sidebands at $\pm\Delta\omega$ in $S_\phi(\omega)$. Hence, in the general case ϕ(t) is given by

$$\phi(t) \approx \frac{I_n c_n \sin(\Delta\omega t)}{2 q_{\max} \Delta\omega} \tag{2-32}$$

for $n \neq 0$. For $n=0$, phase is given by (2-29).

Unfortunately, we are not quite done: (2-32) allows us to figure out the spectrum of ϕ(t), but we ultimately want to find the spectrum of the output voltage of the oscillator, which is not quite the same thing. The two quantities are linked through the actual output waveform, however. To illustrate what we mean by this linkage, consider a specific case where the output may be approximated as a sinusoid, so that $v_{out}(t) = \cos[\omega_0 t + \phi(t)]$. This equation may be considered a phase-to-voltage converter; it takes phase as an input, and produces from it the output voltage. This conversion is fundamentally nonlinear because it involves the phase modulation of a sinusoid.

Performing this phase-to-voltage conversion, and assuming “small” amplitude disturbances, we find that the single-tone injection leading to (2-32) results in two equal-power sidebands symmetrically disposed about the carrier

$$P_{SBC}(\Delta\omega) \approx 10 \cdot \log\left(\frac{I_n c_n}{4q_{\max}\Delta\omega}\right)^2 . \tag{2-33}$$

The foregoing result may be extended to the general case of a white noise source

$$P_{SBC}(\Delta\omega) \approx 10 \cdot \log\left(\frac{\frac{\overline{i_n^2}}{\Delta f}\sum_{n=0}^{\infty} c_n^2}{4q_{\max}^2\Delta\omega^2}\right). \tag{2-34}$$

Equation (2-33) implies both upward and downward frequency translations of noise into the noise near the carrier, as illustrated in Fig. 2.18. This figure summarizes what the foregoing equations tell us: components of noise near *integer multiples* of the carrier frequency all fold into noise near the carrier itself.

Noise near dc gets *upconverted*, weighted by coefficient , so 1/*f* device noise ultimately becomes 1/f^3 noise near the carrier; noise near the carrier stays there, weighted by ; and white noise near higher integer multiples of the carrier undergoes *downconversion*, turning into noise in the 1/f^2 region. Note that the 1/f^2 shape results from the integration implied by the step change in phase caused by an impulsive noise input. Since an integration (even a time-varying one) gives a white voltage or current spectrum a 1/*f* character, the power spectral density will have a 1/f^2 shape.

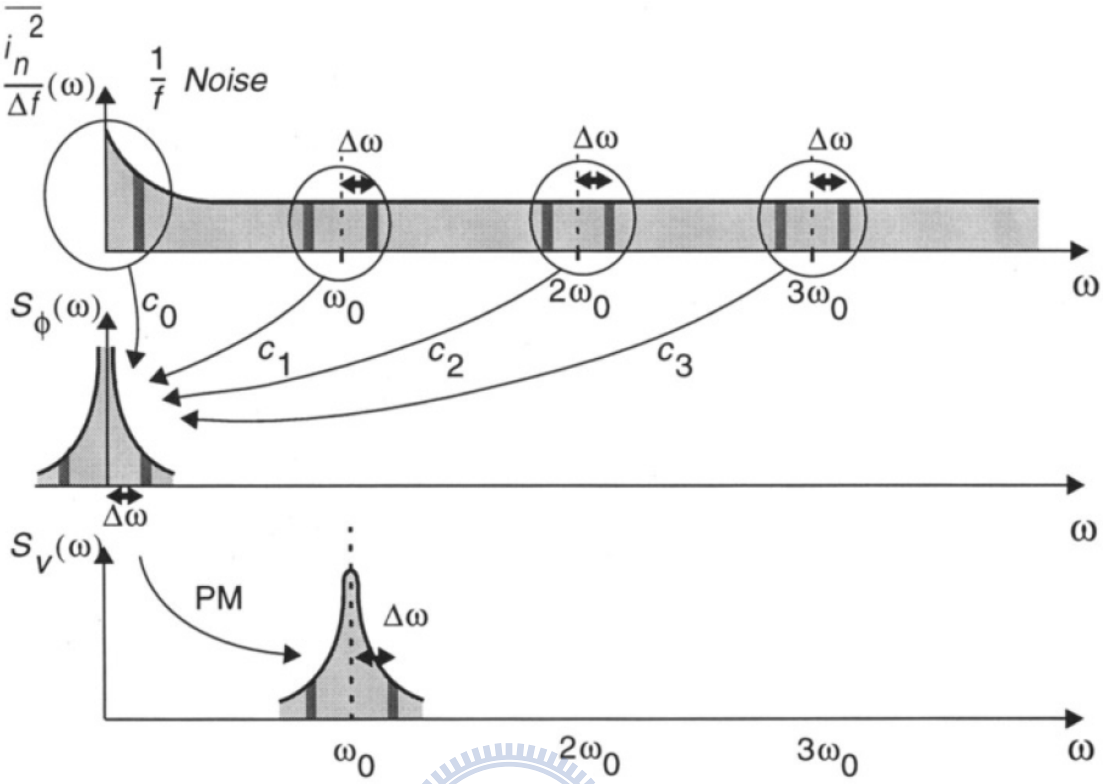

Figure 2.18 Evolution of circuit noise into phase noise.

It is clear from Fig. 2.18 that minimizing the various coefficients c_n (by minimizing the ISF) will minimize the phase noise. To underscore this point quantitatively, we may use Parseval's theorem to write

$$\sum_{n=0}^{\infty} c_n^2 = \frac{1}{\pi}\int_0^{2\pi} |\Gamma(x)|^2 dx = 2\Gamma_{rms}^2 \tag{2-35}$$

so that the spectrum in the $1/f^2$ region may be expressed as

$$L(\Delta\omega) = 10\cdot\log\left(\frac{\frac{\overline{i_n^2}}{\Delta f}\Gamma_{rms}^2}{2q_{\max}^2\Delta\omega^2}\right) \tag{2-36}$$

where Γ_{rms} is the rms value of the ISF. All other factors held equal, reducing Γ_{rms} will reduce the phase noise at all frequencies. Equation (2-36) is the rigorous equation for the $1/f^2$ region and is one key result of the LTV model. Note that no empirical curve-fitting parameters are present in (2-36).

Chapter 3 *Advanced Designs of Related Works*

3.1 Spiral Inductances

In circuit design, we often choose spiral inductances. There are two advantages of using the spiral inductance. The first is that it can easily select the most suitable inductance from the factory's model. The second is the spiral inductance can provide lower noise. However, it also has some shortcomings. (1) The planar spiral inductance value is proportional to the area. Therefore, when we need a higher inductance value, we must use a large chip size. (2) In the standard CMOS process, the quality factor of spiral inductances is usually low. (3) When we use two or more inductors, which has the coupling effect between each other. That will influence the inductance value, quality factor and cutoff frequency. These effects will lead to frequency offset and large noise. (4) Designing a VCO with spiral inductances can not achieve wide tunable range.

3.2 Active Inductances

The following describes the design method of active inductances and discusses the inductance value and quality factor.

3.2.1 The basic concept of active inductor

An active inductance can be realized by using the gyrator and a capacitor. By rotating the phase to 180- degree, the capacitor shows inductive. Using two back-to-back operational transconductance amplifier (OTA) to achieve the gyrator (Fig. 3.1). G_{m1} and G_{m2} represent two OTA's transconductance respectively, and C_p is the parasitic capacitance.

Using this gyrator to achieve an active inductance, and use of Kirchhoff's voltage law to calculate the inductance value. We can see the inductance value and transconductor are related by the formula (3). The inductance value can be increased as the transconduction decrease or the capacitor increase.

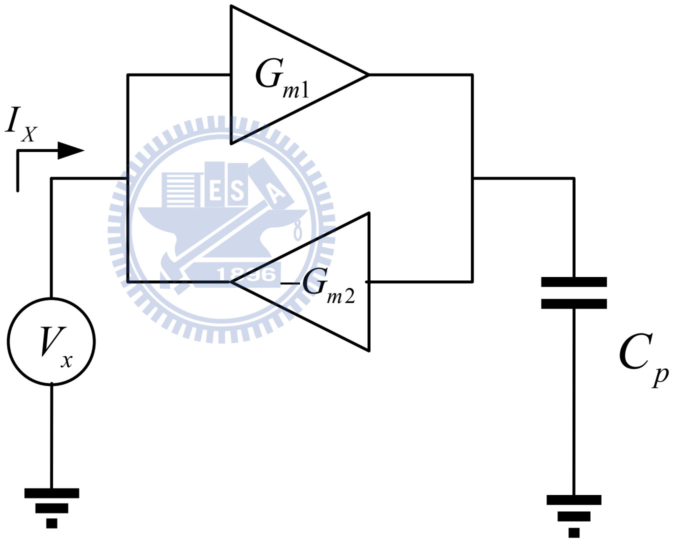

Figure 3.1 Schematic diagram of active inductor

$$-I_x = -G_{m2}(G_{m1}V_x \times \frac{1}{sC_p}) \tag{3-1}$$

$$\frac{V_x}{I_x} = \frac{sC_p}{G_{m1}G_{m2}} = sL_{eq} \tag{3-2}$$

$$L_{eq} = \frac{C_p}{(G_{m1} \cdot G_{m2})} \tag{3-3}$$

3.2.2 Active inductor architecture introduced

A. The general structure

Fig. 3.2 shows the general structure of active inductor and its equivalent circuit.

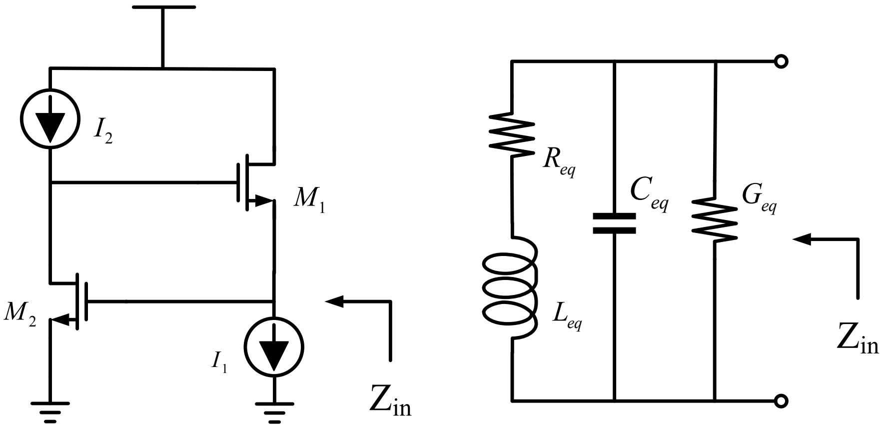

(a) (b)

Figure 3.2 The structure of active inductor and its equivalent circuit.

The input impedance can be derived by the small-signal analysis, shown as follows:

$$Z_{in} \approx \frac{s(C_{gs2}+C_{gd1}+C_{gd2})+g_{ds1}}{(sC_{gd2}+g_{ds2}+g_{m1})(s\cdot(C_{gs2}+C_{gd})+g_{m2})} \tag{3-4}$$

Because C_{gs} is much larger than C_{gd}, so the formula (3-4) can be simplified to

$$Z_{in} \approx \frac{sC_{gs2}+g_{ds1}}{(sC_{gd2}+g_{ds2}+g_{m1})(sC_{gs2}+g_{m2})} = \mathrm{Re}(Z_{in})+j\,\mathrm{Im}(Z_{in}) \tag{3-5}$$

The Z parameter can be converted to Y parameters. The Y_{in} is given by

$$Y_{in} = (Z_{in})^{-1} \approx g_{ds2}+g_{m2}+sC_{gs1}+\frac{g_{m1}g_{m2}}{sC_{gs2}+g_{ds1}} \tag{3-6}$$

The Y_{in} can be approximated by the equivalent circuit model of the active inductor, as shown in Fig 3.2(b), where

$$R_{eq} = \frac{g_{ds1}}{g_{m1} g_{m2}} \tag{3-7}$$

$$L_{eq} = \frac{C_{gs2}}{g_{m1} g_{m2}} \tag{3-8}$$

$$C_{eq} = C_{gs1} \tag{3-9}$$

$$G_{eq} = g_{ds2} + g_{m2} \tag{3-10}$$

B. The cascade structure

Fig. 3.3 shows the general structure of active inductor and its equivalent circuit.

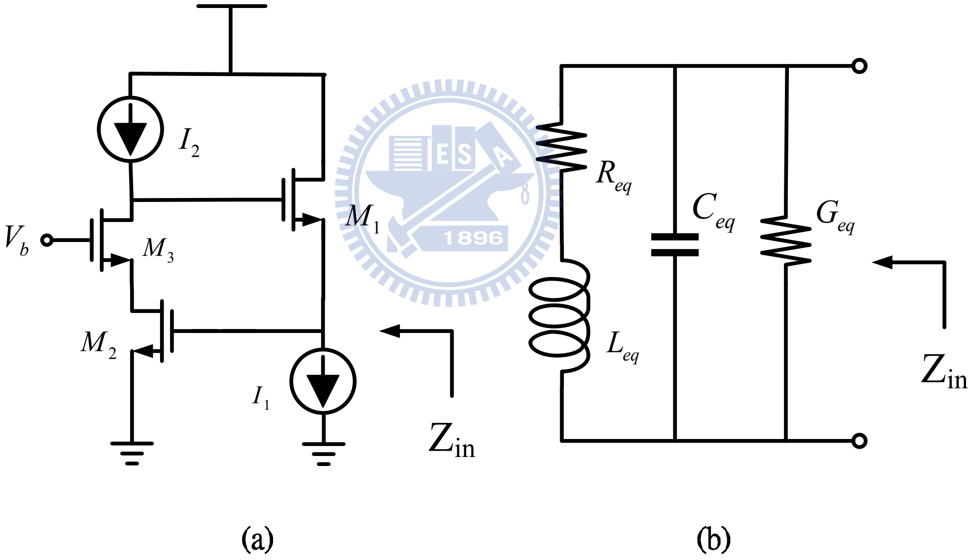

Figure 3.3 The cascade structure of active inductor and its equivalent circuit.

The Y_{in} can be approximated by the equivalent circuit model of the active inductor, as shown in Fig 3.3(b), where

$$R_{eq} = \frac{g_{ds1} g_{ds3}}{g_{m1} g_{m2} g_{m3}} \tag{3-11}$$

$$L_{eq} = \frac{C_{gs2}}{g_{m1} g_{m2}} \tag{3-12}$$

$$C_{eq} = C_{gs1} \tag{3-13}$$

$$G_{eq} = \frac{1}{g_{m2}} \tag{3-14}$$

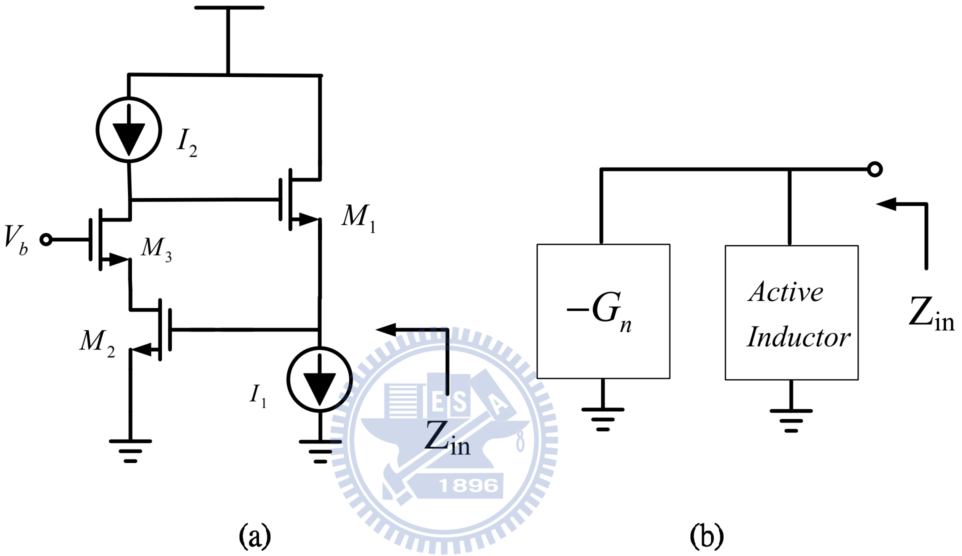

Figure 3.4 Use the transistor M_3 to increase the quality factor.

The transistor M3 increases the characteristic of positive feedback. Therefore, the circuit can be equivalent to an active inductor in parallel to a conductance -G_n (Fig 3.4(b)). The quality factor also can be increased as the conductance G_{eq} decrease. In addition, the transistor M3 provides the functions of gain-boosting. V_b is the control voltage, which can affect the value of transconductance. In this structure, the capacitance part is replaced by the parasitic capacitance of transistors. Therefore, this circuit does not need to include an additional MIM capacitor.

C. Adding feedback resistors for the general structure

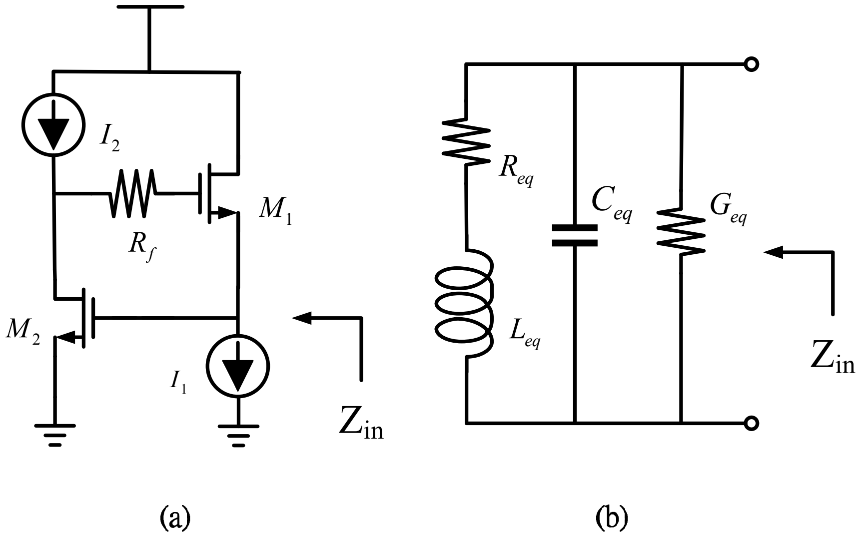

Figure 3.5 Adding feedback resistors for the general structure of active inductor and its equivalent circuit.

The Y_{in} can be approximated by the equivalent circuit model of the active inductor, as shown in Fig 3.5(b), where

$$R_{eq}=\frac{g_{ds1}}{g_{m1}g_{m2}} \tag{3-15}$$

$$L_{eq}=\frac{C_{gs2}(1+g_{ds1}R_f)}{g_{m1}g_{m2}} \tag{3-16}$$

$$C_{eq}=C_{gs1} \tag{3-17}$$

$$G_{eq}=g_{ds2}+\frac{g_{m1}}{1+g_{ds1}R_f} \tag{3-18}$$

Equation (3-16) and Equation (3-18) showed that adding the feedback resistance will lead to reduction of the conductance and the equivalent inductance value increases. Therefore, Adds the feedback resistor can effectively enhance the quality factor of active inductance.

3.2.3 Advantages and disadvantages of active inductor

We can find some advantages of active inductors. (1) The die area is really small. (2) It does not have the coupling effect. (3) The quality factor is very high. (4) Designing a VCO with active inductances can achieve wide tunable range. However, it also has some disadvantages, such as high noise and high power consumption.

Chapter 4 *Proposed Wide tuning range VCO*

4.1 INTRODUCTION

In recent years, rapid growth of wireless communication markets has led to multiple wireless standards. These wireless standards may coexist on the same frequency; therefore, the hardware reused for multiple standards becomes an important issue. In order to solve this problem, the wide tuning range VCO is essential. In the past research, LC-tank VCOs with spiral inductors and varactors are the most used for circuit implementation at radio frequencies. This structure of the tuning frequency depends entirely on the varactor's tunable range; therefore, subject to the influence of traditional CMOS process, the tuning range is limited to less than 30% [1]- [3] making it unattractive for wideband applications. Many ways have been proposed to improve the tuning range of the LC-tank VCO by switched capacitors [4], [5]. To operate at multiple frequencies, a number of switched -capacitor converters for VCO are used. Though the tuning range can be improved, the overall circuit area has increased considerably.

To overcome the increase in chip size, the structure of active inductors has been introduced [6]. An active inductor can be realized by using two gyrators and a capacitor. By rotating the phase to 180- degree, the capacitor shows inductance. Using this active inductor to replace the spiral inductor of LC- tank VCO can effectively reduce the chip area. However this is a one-port inductor topology, so to completely replace the spiral inductor, the active inductor must use more than four transistors, and using more transistors will lead to the increased of the noise on the circuit significantly.

In this chapter, a wide tuning range VCO circuit is proposed. Using differential active inductors and adding a feedback resistor to the variable conductance can achieve the effect of broadband and smaller chip area. The proposed VCO is validated by an implementation using the TSMC 0.18 μm 1P6M process.

4.2 Differential Active Inductors

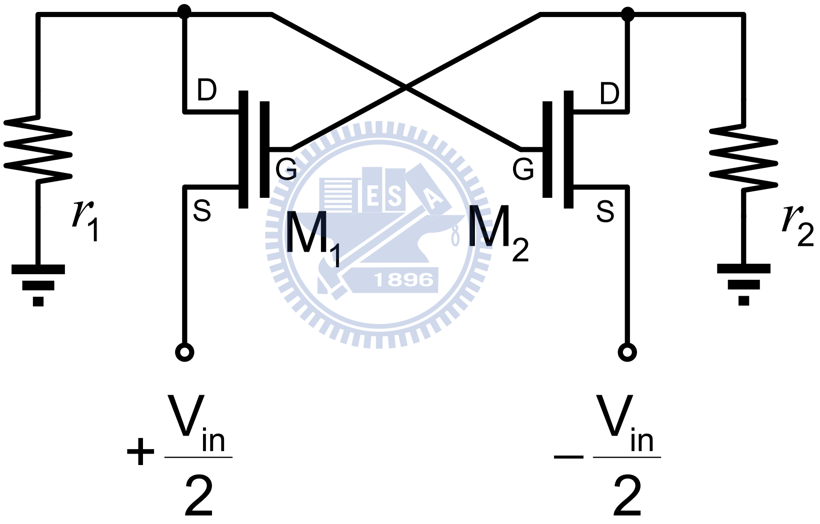

Figure 4.1 The differential active inductor.

When the input signal with the opposite sign ($+V_{in}/2$ and $-V_{in}/2$) is also applied to each of M_1 and M_2 source (Fig 4.1), the Input impedance can be shown as an inductor. In order for the inductor value can be adjusted. The transistor is used as a tunable resistor, using it to replace the fixed resistor. Fig 4.2 shows the transistor is used as a tunable resistor. When the gate voltage is tuned, the drain- to-source impedance is equivalent to a tunable resistor.

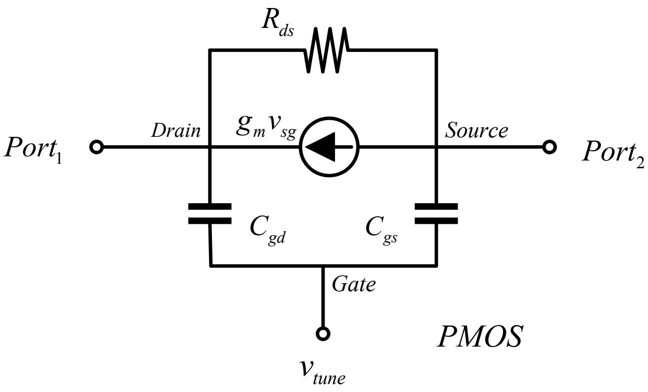

Figure 4.2 The transistor is used as a tunable resistor.

Fig 4.3 shows the VCO with active inductor. Because the VCO's tuning range depends on the tunable range of active inductor. Therefore, using this active inductor can achieve a wide tuning range VCO.

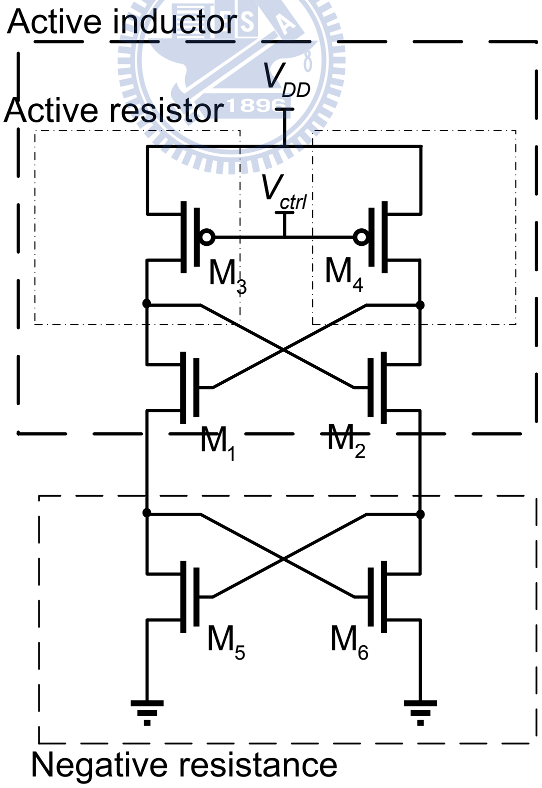

Figure 4.3 The VCO with the active inductor.

Through simulation (Fig 4.4), we found a problem. When the control voltage is gradually increased to a specific value, the negative resistor device of VCO can not work.

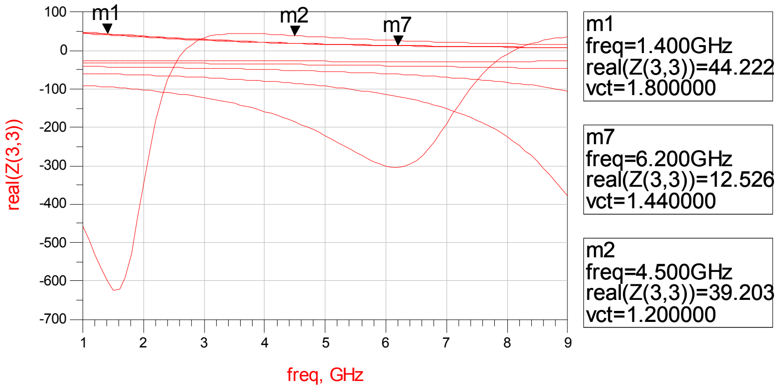

Figure 4.4 Simulation output negative resistance value

In order to solve this problem, we adds a feedback resistor in the tunable reisitor (Fig 4.5). The feedback resistor can limit the maximum value of the tunable reisitor.

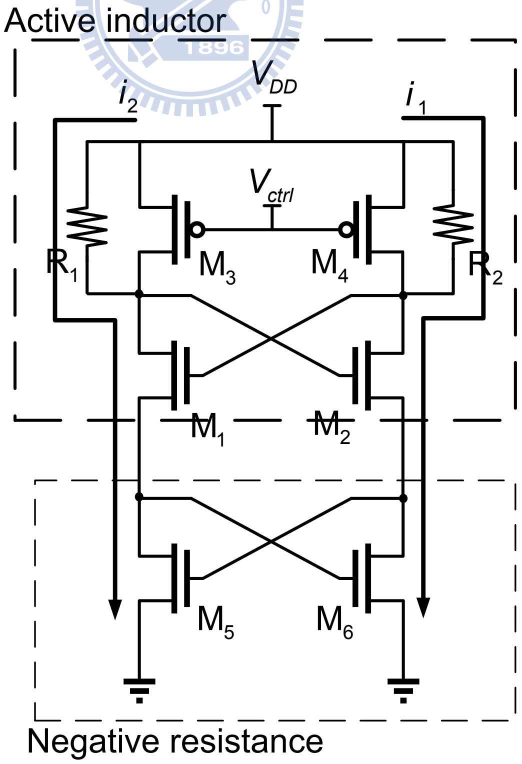

Figure 4.5 Adding feedback resistors in the active inductor.

Simulation again (Fig 4.6), the tunable range of the control voltage shows an increase of 0.7V.

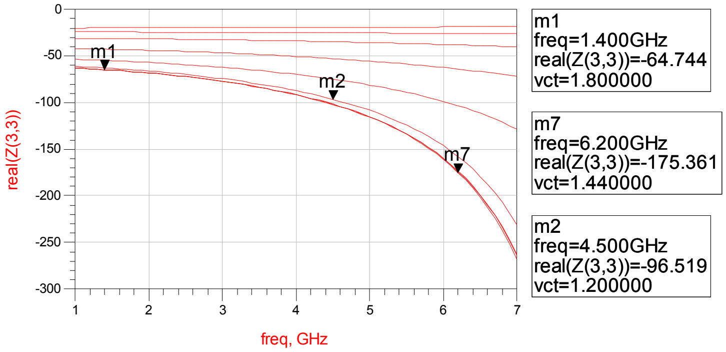

Figure 4.6 Simulation output negative resistance value

4.3 Circuit Design and Analysis

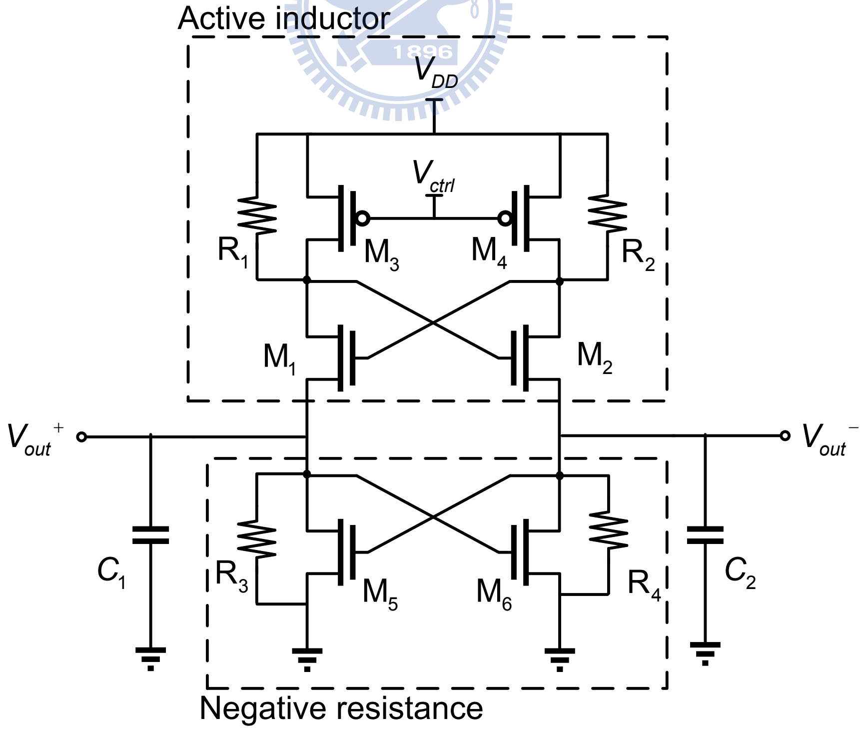

Figure 4.7 Proposed VCO circuit.

Our design is shown in Fig 4.7. The tunable active inductor is implemented by transistors M_1-M_4, where the gyrator-C architecture is adopted to emulate the characteristics of an inductor. The proposed two-port circuit topology compared to the conventional one-port active inductor uses fewer transistors, thus reducing the impact of noise on the circuit, and the chip area becomes smaller. Adding a resistor in parallel to the transistor's (M_1-M_4) source to the drain, effectively improves the tunable range of V_{ctrl}. Fig 4.8 shows the small-signal equivalent circuit of the active inductor (M_1-M_4 and R_1-R_2) in Fig 4.7. M_1 and M_2 form a cross-coupled pair, while the combination of M_3 and R_1 is modeled as g_1, and the combination of M_4 and R_2 is modeled as g_2.

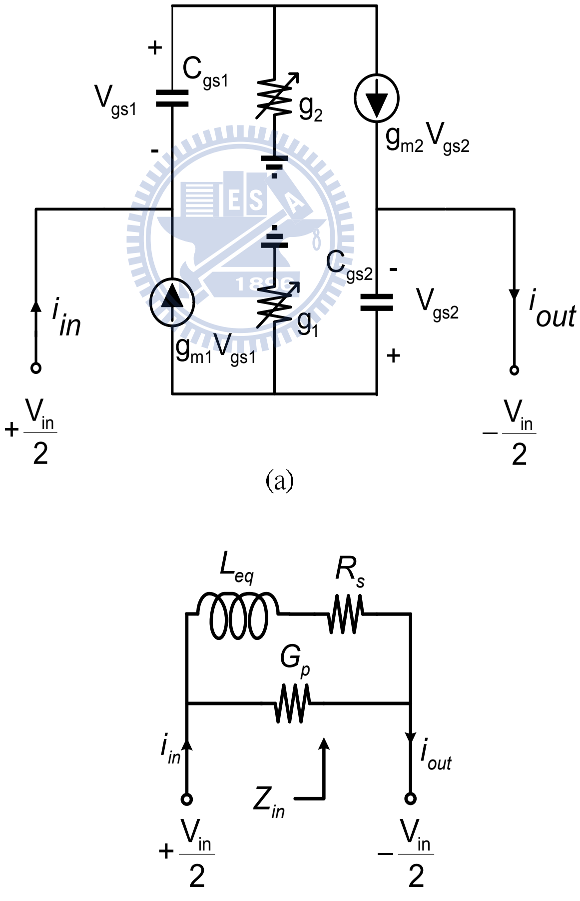

(a)

(b)

Figure 4.8 (a) Small-signal equivalent circuit of the differential active inductor.
(b) Simplified circuit model of the active inductor.

When the input signal with the opposite sign (+$V_{in}/2$ and -$V_{in}/2$) is also applied to each of M_1 and M_2 source, the input impedance can be derived by the small-signal analysis, shown as follows:

$$Z_{in} \equiv \frac{v_{in}}{i_{in}} = \frac{2(j\omega C_{gs1} + g_2 - g_{m2})}{g_2(j\omega C_{gs1} + g_{m1})} \tag{4-1}$$

As $g=g_1=g_2$ and $g_m=g_{m1}=g_{m2}$ the input impedance can be approximated by the simplified circuit model of the active inductor, as shown in Fig 4.8(b), where

$$L_{eq} = \frac{2C_{gs1}}{g(2g_m - g)} \tag{4-2}$$

$$R_s = \frac{2(g - g_m)}{g(2g_m - g)} \tag{4-3}$$

$$G_P = \frac{g_m}{2} \tag{4-4}$$

The equation (4-2) shows that the equivalent inductance value depends on the circuit parameters, including C_{gs1}, g_m, and g, and tuning conductance g can do the most effective inductance adjustment. Therefore, a wide tunable range of the variable conductance was proposed by adding a feedback resistance of PMOS (Fig 4.9).

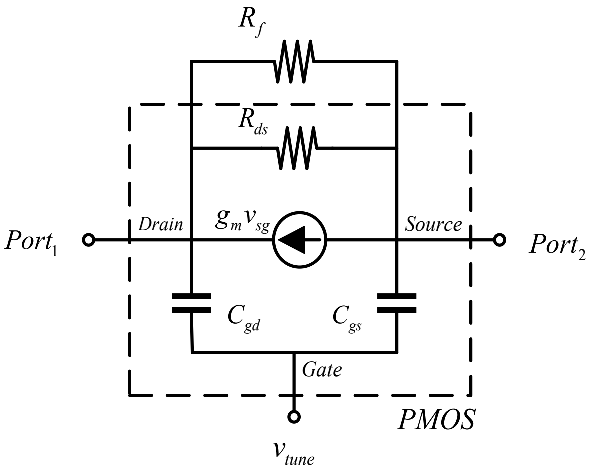

Figure 4.9 Tunable conductance two port equivalent model

The drain-source port can be equivalent to a variable conductivity by adjusting the gate voltage V_{ctrl}. However the negative resistance in the VCO will lose efficiency. This is because the increase of V_{ctrl}, the conductance becomes smaller to a certain value which leads to lack of supply current. So adding the feedback resistor R_f to limit the minimum value of the variable conductance can effectively solve this problem and improve the tunable range of V_{ctrl}.

In phase noise analysis, the pioneering work by Hajimiri and Lee is applied to evaluate the phase noise L of the circuit at an offset frequency $\Delta\omega$ from the carrier [10]. The phase noise is given by

$$L(\Delta\omega) = 10\log(\frac{\overline{i_n^2}\Gamma_{rms}^2}{2\Delta\omega^2 C_{eq}^2 A_{\tan k}^2}) \tag{4-5}$$

with C_{eq} being the tank capacitance. A_{tank} is the oscillation amplitude across the resonator and Γ_{rms} is the root mean square value of the impulse sensitivity function (ISF). Equation (4-5) shows that a larger C_{eq} can lead to a lower phase noise. Fig 4.7, varactors were replaced by C_1 and C_2, thereby increasing the tank capacitance C_{eq} thus lowering the phase noise.

4.4 Simulated Results

(1)Tuning Range

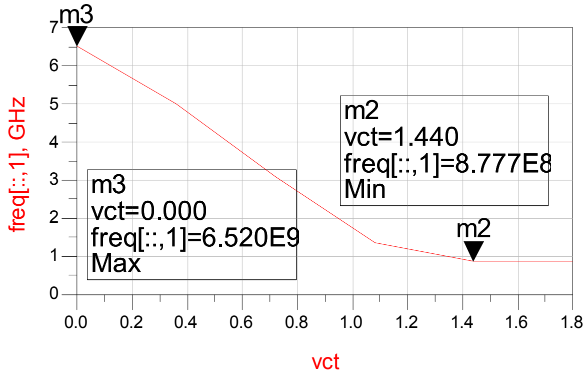

(2)Phase Noise

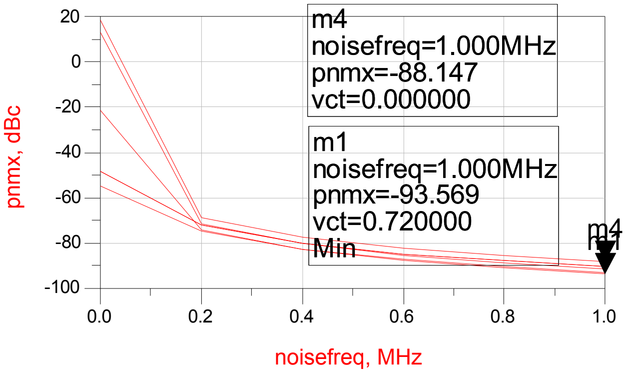

(3)Output Power

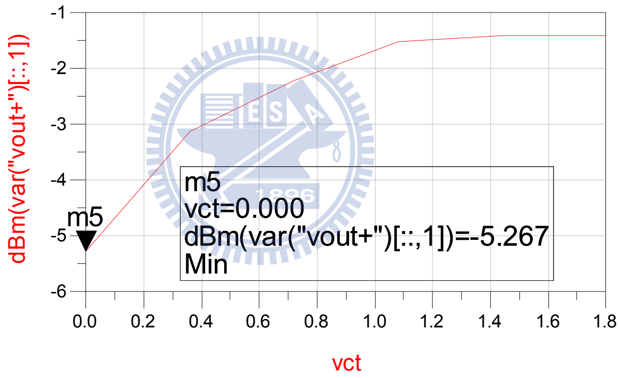

(4)Tuning Sensitivity

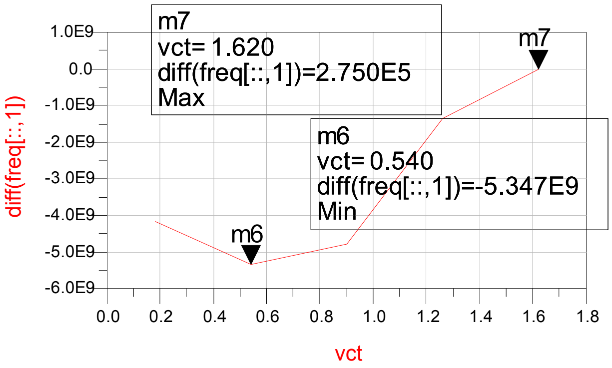

(5) CornerCase(TT、FF、SS、FS、SF)　Temperature=25°C

RF Corner	TT	FF	SS	FS	SF
Oscillator Frequency (GHz)	0.8~ 6.5	1.3 ~ 7.1	0.88 ~ 5.9	1.2 ~ 5.7	0.92 ~ 5.8
Phase Noise (dBc/Hz@1MHz)	-88 ~ -93	-88 ~ -94	-89 ~ -94	-91 ~ -94	-89 ~ -94
Output Power (dBm)	-5.26	-5.4	-5.5	-4.15	-3.8
Power Consumption (**m**W)	19.8	24.3	22.6	21.2	23.6
Tuning Range (%)	152	138	148	130	145

(6) Temperature effect

Temperature	-50℃	25℃	80℃
Oscillator Frequency (GHz)	0.86 ~ 6.2	0.8 ~ 6.5	0.9 ~ 5.4
Phase Noise (dBc/Hz@1MHz)	-88 ~ -94	-88 ~ -93	-89 ~ -94
Output Power (dBm)	-4.6	-5.26	-5.5
Power Consumption (**m**W)	19.8	19.8	18.72
Tuning Range (%)	151	152	142

(7) Voltage variation

VDD	1.76	1.78	1.8	1.82	1.84
Oscillator Frequency (GHz)	0.7~ 6.45	0.8 ~ 6.48	0.8 ~ 6.5	0.9 ~ 6.55	0.9 ~ 6.59
Phase Noise (dBc/Hz@1MHz)	-88 ~ -93	-88 ~ -93	-88 ~ -93	-88 ~ -93	-88 ~ -93
Output Power (dBm)	-6	-5.6	-5.26	-4.97	-4.72
Power Consumption (**m**W)	18.48	19.22	19.8	20.56	21.34
Tuning Range (%)	156	155	152	150	149

4.5 Measured Results

Fig 4.10 shows the die microphotograph of the proposed VCO, where it is fabricated by using the TSMC 0.18 μm CMOS process.

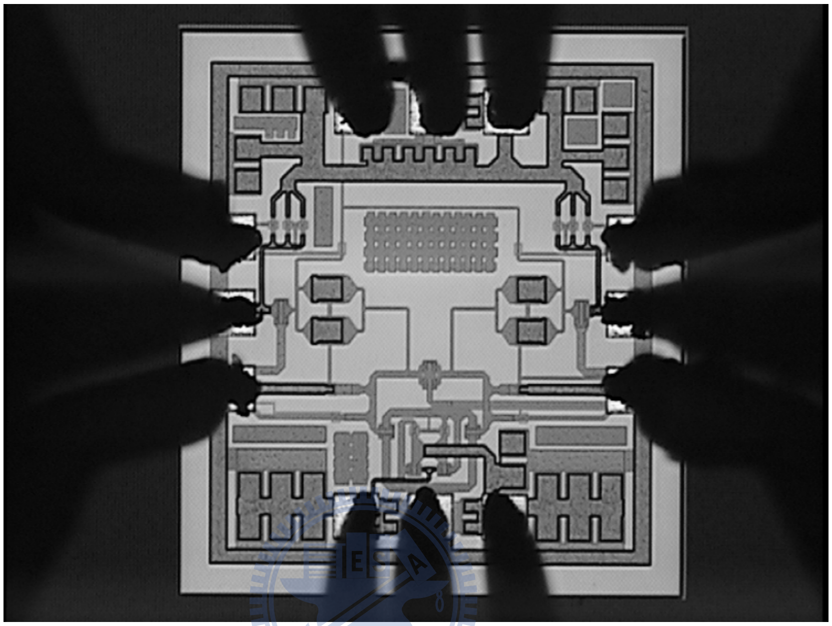

Figure 4.10 Microphotograph of the proposed VCO.

The total die area is $0.60 \times 0.67 mm^2$ including the pads, where the core of active area is only $175 \times 170 \mu m^2$. The circuit characteristics of the VCO were evaluated through on-wafer probing. The circuit operates at a supply voltage of 1.8 V. The measured output oscillation frequencies are shown in Fig 4.11. As the controlled voltage is tuned from 0 to 1.8 V, the proposed VCO provides an output frequency from 0.5 GHz to 5.6 GHz with an enough output power of – 6 dBm. The worst power consumption of the VCO core is 17.8 mW. Fig 4.12 shows the phase noise at 1-MHz offset when V_{ctrl} sweeps is tuned from 0.1 to 1.8 V.

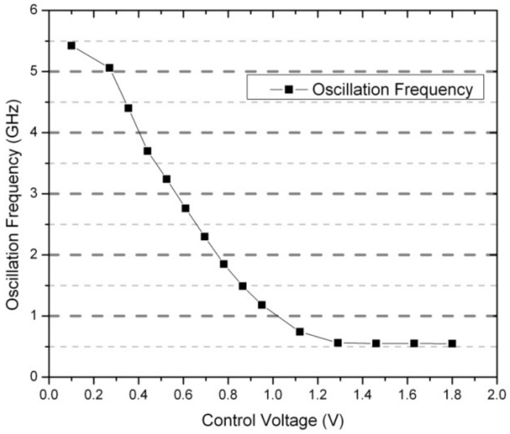

Figure 4.11 The tuning range of the VCO.

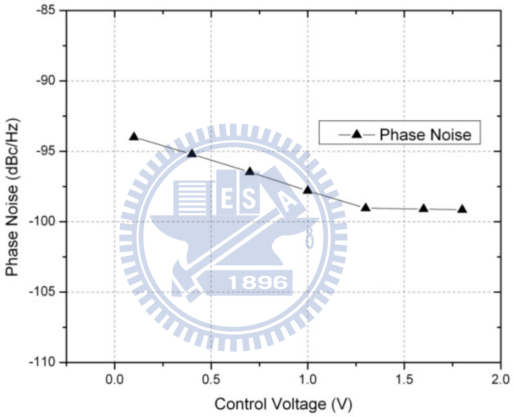

Figure 4.12 The phase noise of the proposed VCO.

When the VCO is operates at an oscillation frequency of 538 MHz, the output power and the phase noise at 1-MHz offset are -5.7 dBm and -99 dBc/Hz. When the oscillation frequency is 5.6 GHz, the output power and the phase noise at 1-MHz offset are 0.4 dBm and -94 dBc/Hz. Comparison results show that our proposed work yields ultra wide tuning range, small chip size and maintain an appropriate phase noise.

4.6 Measured Performance Summary and Comparison

TABLE I

Wide Tuning-Range VCO MEASURED PERFORMANCE SUMMARY AND COMPARISON

Ref.	CMOS Technology (μm)	Tuning		Phase Noise @ 1MHz offset(dBc/Hz)	P_{DC} (mW)	Active Area (μm^2)
		GHz	%			
[7]	0.18	3.8 ~ 7.4	64	-75. ~ -92	29.1	-
[8]	0.18	0.5 ~ 2	120	-78 ~ -90	13.8	300x300
[9]	0.18	0.4 ~ 1.6	120	-88 ~ -95	26	-
[10]	0.18	2.7 ~ 5.4	66	-90 ~ -95	18.4	600x700[b]
[11]	0.18	1.85 ~ 3.66	65	-81 ~ -111[a]	21.6	-
This work	0.18	0.54 ~5.67	165	-94 ~-99	17.8	175x170

[a] PN at 3MHz offset [b] including pads and guard ring

Chapter 5 *Conclusion*

An ultra-wide tuning range VCO of 5 GHz is proposed. This VCO uses differential active inductor architecture, and adds a feedback resistor in the active inductor. The feedback resistor can limit the minimum value of conductivity. The circuit current is sufficient, because of small conductance. Therefore, the tuning range of VCO can be increased. This structure requires less number of transistors, thus, the chip size can be smaller. The proposed circuit is implemented by the TSMC 0.18μm 1P6M process technology and the measurement result of the proposed VCO shows an output frequency from 0.5 GHz to 5.6 GHz. The tunable frequency range can reach a bandwidth of 5GHz, and the tuning range is 165%. The worst phase noise measurements at 1 MHz offset frequency is -94 dBc/Hz. Using the active inductor, the die area of the VCO is 175 x 170 μm^2.

REFERENCES

[1] IEEE 802.16e/D12-2005, "IEEE Standard for Local and Metropolitan Area Networks - Part 16: Air Interface for Fixed Broadband Wireless Access Systems - Amendment for Physical and Medium Access Control Layers for Combined Fixed and Mobile Operation in Licensed Bands," Oct. 2005.

[2] D. B. Lesson, "A simple model of feedback oscillator noise spectrum," *Proc. IEEE,* vol. 54, pp. 329-330. Feb. 1966.

[3] B. Min and H. Jeong, "5-GHz CMOS *LC* VCOs with wide tuning ranges," *IEEE Microw. Wireless Compon. Lett.*, vol. 15, no. 5, pp. 336–338, May 2005.

[4] R. S. Rana, X. D. Zhou, and Y. Lian, "An optimized 2.4 GHz CMOS *LC*-tank VCO with 0.55%/V frequency pushing and 516 MHz tuning range," in *IEEE Int. Circuits Syst. Symp.*, May 2005, pp. 4811–4814.

[5] B. De Muer, N. Itoh, M. Borremans, and M. Steyaert, "A 1.8-GHz highly-tunable low-phase-noise CMOS VCO," in *IEEE Custom Integr.Circuits Conf.*, May 2000, pp. 585–588.

[6] D. Berny, A. M. Niknejad, and R. G. Meyer, "A 1.8-GHz *LC* VCO with 1.3-GHz tuning range and digital amplitude calibration," *IEEE J. Solid-State Circuits*, vol. 40, no. 4, pp. 909–917, Apr. 2005.

[7] ——, "A wideband low-phase-noise CMOS VCO," in *IEEE Custom Integr. Circuits Conf.*, Sep. 2003, pp. 555–558.

[8] J.-S. Ko and K. Lee, "Low power, tunable active inductor and its applications to monolithic VCO and BPF," in *IEEE MTT-S Int. Microw.Symp. Dig.*, Jun. 1997, pp. 929–932.

[9] Hajimiri and T. H. Lee, "A general theory of phase noise in electrical oscillators," *IEEE J. Solid-State Circuits*, vol. 33, no. 2, pp. 179–194, Feb. 1998.

[10] Hajimiri and T. H. Lee, "A general theory of phase noise in electrical oscillators," *IEEE Journal of Solid-State Circuits*, vol. 33, no. 2, pp. 179- 194, Feb. 1998.

[11] Mehrabian, M.; Nabavi, A.; Rashidi, N., "A 4~7GHz ultra wideband VCO with tunable active inductor," *Ultra-Wideband, 2008. ICUWB 2008. IEEE International Conference on* , vol.2, no., pp.21-24, 10-12 Sept. 2008

[12] R. Mukhopadhyay, Y. Park, P. Sen, N. Srirattana, J. Lee, C.-H. Lee, S. Nuttinck, A. Joseph, J. D. Cressler, and J. Laskar, “Reconfigurable RFICs in Si-based technologies for a compact intelligent RF frontend, ”*IEEE Trans. Microw. Theory Tech.*, vol. 53, no. 1, pp. 81–93, Jan. 2005.

[13] Y.-H. Chuang, S.-L. Jang, J.-F. Lee, and S.-H. Lee, “A low voltage 900 MHz voltage controlled ring oscillator with wide tuning range,” in *IEEE Asia–Pacific Circuits Syst. Conf.*, Dec. 2004, pp. 301–304.

[14] Chien-cheng Wei, Hsien-chin Chiru and Wu-Shiung Feng, “An Ultra-WideBand CMOS VCO with 3-5GHz Tuning range”, IEEE international workshop on radio frequency technology, 2005 Singapore.

[15] Huang, G.; Kim, B.-S., "Programmable active inductor-based wideband VCO/QVCO design," *Microwaves, Antennas & Propagation, IET* , vol.2, no.8, pp.830-838, December 2008

[16] B. Razavi, *Design of Analog CMOS Integrated Circuits*, McGRA-Hill, 2001.

[17] 詹豐吉，<低功率、低相位雜訊之雙頻帶電壓控制振盪器設計>，國立交通大學電信工程研究所碩士論文，2007 年。

[18] 黃俊諺，<全積體化低電壓低功率之 CMOS 電壓控制振盪器設計>，國立交通大學電信工程研究所碩士論文，2008 年。

[19] 李明宗，<低功率和低電壓之電壓控制振盪器設計>，國立交通大學電信工程研究所碩士論文，2009 年。

[20] 李威璁，<射頻主動式電感的實現與應用>，國立交通大學電信工程研究所碩士論文，2008 年。